Wiley
Journal of Engineering
Volume 2025, Article ID 8829522, 15 pages
https://doi.org/10.1155/je/8829522

WILEY

Research Article

Crashworthiness Research Based on Lightweight Bus of Honeycomb Sandwich Body

Yi Pang,[1,2] Shaw Voon Wong,[1,3] Yong Han,[2] Yahaya bin Ahmad,[3] Kean sheng Tan,[4] Azizan As'arry,[1] Sai Zhang,[5] and Pengfei Ren[5]

[1]*Universiti Putra Malaysia, Serdang, Malaysia*
[2]*Xiamen University of Technology, Xiamen, China*
[3]*Malaysian Institute of Road Safety Research, Kajang, Malaysia*
[4]*National Defense University of Malaysia, Kuala Lumpur, Malaysia*
[5]*China Automotive Technology and Research Centre, Tianjin, China*

Correspondence should be addressed to Shaw Voon Wong; wongsv@upm.edu.my

Received 19 February 2025; Revised 28 August 2025; Accepted 3 October 2025

Academic Editor: Shikha Binwal

To enhance the lightweight design and structural safety of electric buses, this study focused on optimizing the chassis stress-bearing beam structure for frontal impacts and applying honeycomb sandwich materials to the bus body structure, particularly for improving rollover crashworthiness. High-speed tensile and compression tests were performed to characterize the dynamic mechanical behavior of key materials, and the resulting data were used to develop high-fidelity material models. These models significantly improved the accuracy and reliability of the simulations. The optimized structural design was validated through physical testing, confirming compliance with both frontal and rollover safety standards. Compared to conventional steel or aluminum body structures, the use of honeycomb sandwich materials resulted in a weight reduction of approximately 500 kg. Notably, the honeycomb sandwich structure played a critical role in maintaining structural stability and occupant survival space during rollover events. This study demonstrates the effectiveness of honeycomb sandwich materials in achieving lightweight and crashworthy designs for electric bus.

Keywords: dummy injury value; frontal rigid barrier collision; honeycomb sandwich material; lightweight; rollover test

1. Introduction

Automobile safety and lightweight design are two critical indicators in the process of automotive development and design, with structural crashworthiness being a vital core component of automotive safety [1, 2].

In the European Union (EU), approximately 30,000 bus or coach passengers are injured each year. To enhance passenger safety, the EU introduced the ECE R66 regulations in 1995 and updated them in 2005, mandating rollover testing during bus manufacturing. According to ECE R66, the structural integrity of the bus body must satisfy deformation strength certification, and a defined passenger survival space must remain uncompromised after the test [3–5]. Similarly, China issued the national standard GB JT/T 1369-2020 in 2021, titled "Passenger Protection in Frontal Collisions of Passenger Vehicles," which focuses on evaluating and improving the frontal crash safety performance of buses. This regulation outlines technical requirements and testing methods to ensure the protection of drivers and passengers in the frontal area during collision events [6, 7].

Accordingly, the design and development of bus safety systems must conform to both EU and Chinese regulatory frameworks to ensure full compliance. In parallel, extensive research has demonstrated a strong correlation between vehicle lightweighting and energy consumption. Lightweighting is recognized as a key strategy for improving the energy efficiency and driving range of both electric and internal combustion engine vehicles. It involves minimizing vehicle mass while maintaining structural integrity and occupant safety. Studies indicate that a 10% reduction in vehicle weight can reduce fuel consumption in conventional vehicles by approximately 6% to 8% [8, 9], while in electric vehicles, the same reduction can increase driving range by 5% to 8% [10, 11].

According to the Corporate Average Fuel Economy (CAFE) standards, all Original Equipment Manufacturers (OEMs) must meet fuel efficiency targets based on the average weight of their vehicle fleets, making lightweight design a key priority in automotive engineering [12]. Current lightweighting strategies include the use of high-strength lightweight alloys [13–15], porous materials [16–18], substitution of metal components with plastics [19–23], and structural optimization [24–27]. Among these, the development and application of advanced materials and processing technologies-particularly the integration of high-strength magnesium-aluminum alloys in chassis system-have shown greater impact on improving fuel economy and crash safety than structural redesign alone. For example, the 2015 Tesla model employed a fully aluminum alloy body and chassis, incorporating laser welding and friction stir welding, which achieved a 15% weight reduction while maintaining effective energy absorption in frontal collisions [28].

This study, guided by the Chinese national standard GB JTT 1369-2020 for frontal occupant protection and the European rollover regulation ECE-R66, presents a comprehensive investigation into the crash performance of the bus chassis and honeycomb sandwich material body structures. In frontal collisions, the optimization of the chassis longitudinal beam-serving as the primary force transmission path-significantly improved energy absorption and enhanced occupant safety. In rollover collisions, the honeycomb sandwich body structure demonstrated excellent structural stability and energy absorption capacity, effectively preserving the survival space. By replacing traditional steel or aluminum body materials with honeycomb sandwich composites, the bus body weight was reduced by approximately 500 kg, equivalent to a 7% reduction in overall vehicle weight, without compromising structural integrity. This research introduces a novel methodology that integrates structural optimization, lightweight materials, and advanced simulation and testing, offering a valuable reference for the development of crashworthy and energy-efficient electric buses.

2. Methodology for Bus Design

By incorporating honeycomb sandwich materials and utilizing advanced manufacturing techniques in the construction of bus bodies, a substantial reduction in overall vehicle weight can be achieved. Specifically, the application of sandwich structures yields a weight savings of approximately 10 kg per square meter compared to conventional steel materials. Provided that the structural performance of the honeycomb sandwich panels satisfies the safety requirements stipulated in both the European Regulation ECE-R66 and the Chinese Standard GB JT/T 1369-2020, significant lightweighting of the bus can be realized without compromising crashworthiness. This study employs a combination of finite element simulation and experimental validation to guide the lightweight design process, as outlined in the flowchart presented in Figure 1.

First, the dynamic mechanical properties of the sheet and foam materials were characterized through high-speed tensile testing. Subsequently, tests were performed on the sandwich core material, and a corresponding hardening model was developed based on the experimental data. For mechanical performance analysis, appropriate material models from the DYNA software library were selected. To accurately represent structural failure under multi-axial stress conditions typical of collisions, the GISSMO failure model was employed. A full-vehicle finite element model, including the restraint system, was then established to evaluate crash performance. Based on an analysis of the force transmission paths, optimization strategies were proposed, and their effectiveness was validated through physical testing.

3. High-Speed Testing of Honeycomb Sandwich Material

High-speed tensile testing is an experimental method employed to study the mechanical properties of materials. It is commonly used to assess characteristics such as strength, ductility, and fracture behavior. This experiment involves subjecting standardized material specimens to rapid tensile loading to simulate sudden loading or impact loads that may be encountered in real-world applications [29]. To ensure experimental repeatability and support the accuracy of numerical modeling, the materials and geometric parameters of each component in the honeycomb sandwich structure were clearly defined. The sandwich specimens consisted of two outer face sheets made of 1.0-mm-thick glass fiber reinforced epoxy composite laminates and a 20-mm-thick hexagonal aramid paper honeycomb core. The honeycomb structure had a cell diameter of 6.4 mm, wall thickness of 0.1 mm, and an overall density of approximately 30 kg/m^3. The cells were filled with closed-cell polyurethane foam with a density of 60 kg/m^3 to enhance the compressive resistance of the core.

From the honeycomb sandwich material of the bus body, specimens were cut for tensile and compressive testing. As shown in Figure 2, the test specimen of the honeycomb sandwich material consists of two outer layers of rigid material connected by a honeycomb structure in the middle, filled with foam material to resemble a super-enhanced spring structure.

The compression specimens measured 50 mm × 50 mm × 50 mm, as shown in Figure 2. All specimens were precisely cut using CNC waterjet machining to ensure dimensional accuracy and material integrity.

The tensile specimens were designed in a dog-bone shape with a gauge length of 20 mm and a width of 5 mm, as the Figure 3. The high strain rate tensile tests were performed in accordance with the China national standard GB/T 30069.2-2016, High Strain Rate Tensile Test of Metallic Materials-Part 2: Hydraulic Servo-Type and Other

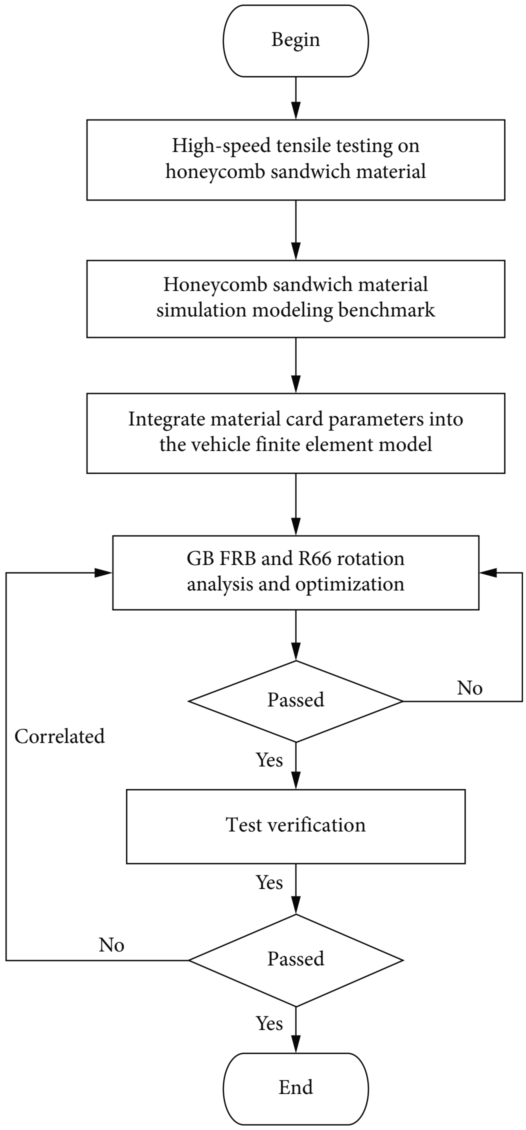

Figure 1: Flowchart of methodology.

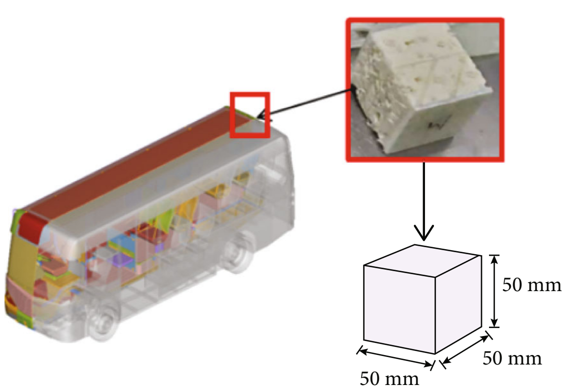

Figure 2: Compression specimen of sandwich material.

Testing Systems, which specifies the procedures and equipment requirements for such dynamic testing.

Specimens for both tension and compression tests were meticulously extracted from the bus body's honeycomb

Figure 3: Tensile specimen of sandwich material.

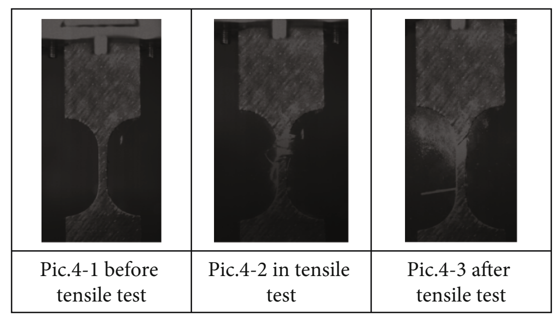

Figure 4: Comparison before and after the tensile test.

sandwich material, then used the German Zwick high-speed dynamic tensile testing machine to conduct test.

During the tensile test, the strain rate of the entire vehicle structure typically ranges from 1 to 100/s. Dynamic tensile tests were conducted on specimens in accordance with the test standards. Tensile experiments were conducted at three distinct strain rates: 1/s, 10/s, and 100/s; all effective experiments were repeated three times to confirm the consistency of the results. Images capturing the specimen both pre- and post-tensile testing are presented Figure 4.

Figure 5 shows the force–displacement curves of tensile tests obtained from samples tested at different strain rates. From the experimental results, it can be observed that at a strain rate of 1/s, the material's peak force is 4200 N, and the fracture displacement is 1.75 mm. As the loading speed increases, the fracture displacement tends to increase, while the peak force remains relatively unchanged. It is necessary to consider the effect of strain rate on the failure parameters in the material card. In addition, three repeated tests were conducted at each strain rate. The statistical results show that at 1/s, the peak force averages about 4150 N with a scatter band of 4100–4200 N, a coefficients of variation (COV) of 1.2%, and a knock-down factor (KDF) of 0.98; the fracture displacement averages 1.65 mm, ranging from 1.60 to 1.70 mm, with a COV of 3.0% and a KDF of 0.95. At 10/s, the peak force averages about 3900 N with a scatter band of 3800–4000 N, a COV of 2.6%, and a KDF of 0.96; the fracture displacement averages 1.72 mm, ranging from 1.60 to 1.80 mm, with a COV of 5.8% and a KDF of 0.91. At 100/s, the peak force averages about 3970 N with a scatter band of 3900–4000 N, a COV of 1.4%, and a KDF of 0.98; the fracture displacement averages 2.73 mm, ranging from 2.40 to

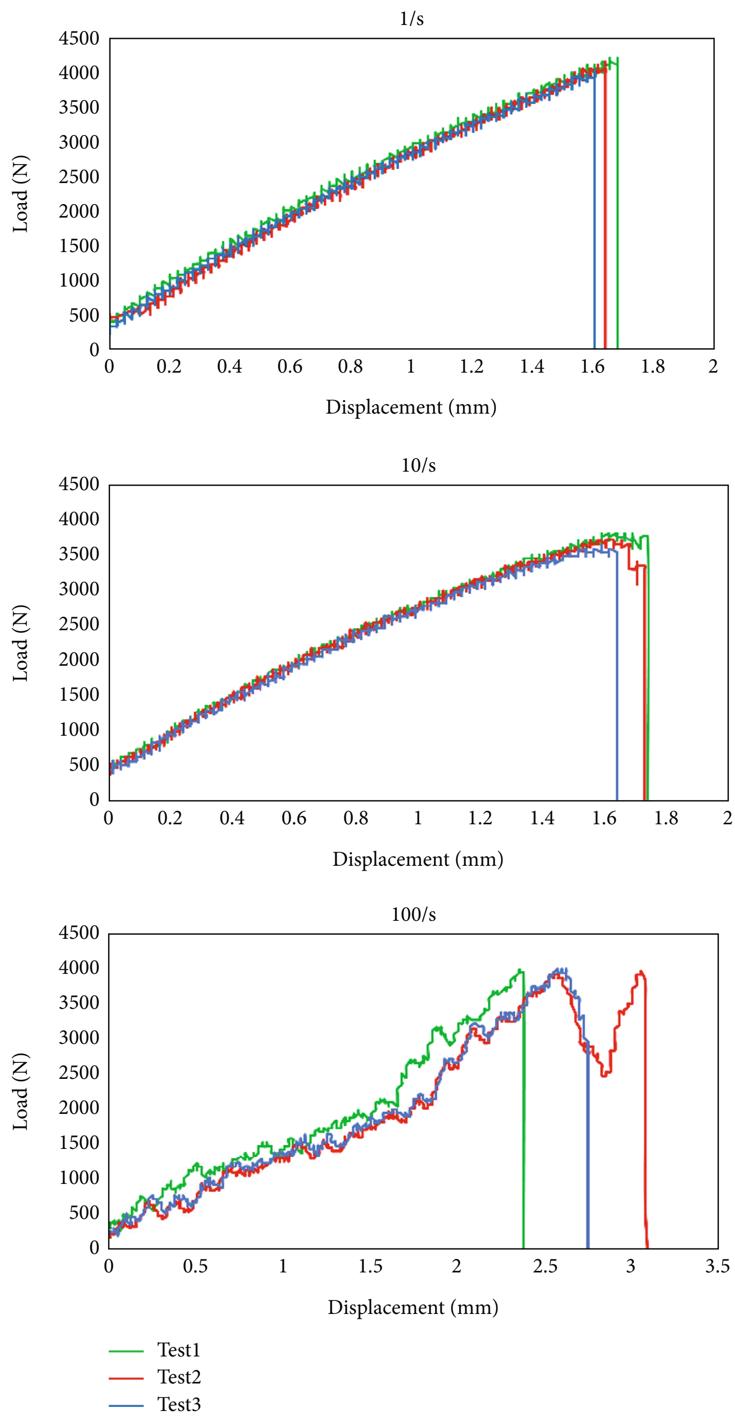

Figure 5: The stress–strain curve in tensile tests.

3.00 mm, with a COV of 11.0% and a KDF of 0.82. Overall, the scatter of peak force is very small (COV generally < 3%), confirming the reliability of the strength results, while the fracture displacement exhibits greater variability at higher strain rates. The KDF calculated based on the lower-bound approach (0.82–0.98) have been adopted for material card calibration to ensure conservative and safe simulations.

Upon completion of the tensile test, the tensile strength performance parameters and the corresponding stress-strain curve will be derived. Subsequently, a compressive test was conducted on the sandwich material sample. Experiments were carried out at three distinct strain rates: 1/s, 10/s, and 100/s, all effective experiments were repeated three times to confirm the consistency of the results. Images capturing the sample both pre(left) and post-compression are presented Figure 6.

The compressive curves, derived from samples subjected to varying strain rates, are illustrated in Figure 7. From the

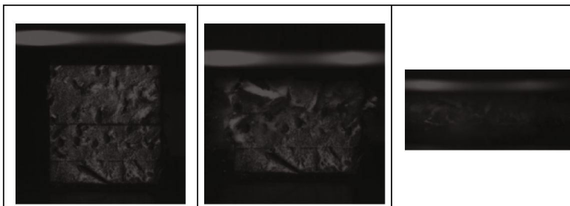

Pic.6-1 before compression test	Pic.6-2 in compression test	Pic.6-3 after compression test

Figure 6: Comparison before and after compressive test.

experimental curve, it can be observed that as the compression displacement increases, the force curve initially exhibits a small peak, after which the force starts to decrease. As the displacement continues to increase gradually, the material undergoes progressive compression, and its resistance to deformation increases. In particular, the peak force measured at approximately 40% compression clearly increases with strain rate: about 14,000 N at 1/s, 15,000 N at 10/s, and 24,000 N at 100/s. The scatter bands of three repeated tests remain narrow, with COV generally below 3%, confirming the stability and reliability of the compressive strength results. Nevertheless, more pronounced fluctuations are observed in the plateau regions at higher strain rates. Based on the lower-bound statistical approach, the KDF were determined to be approximately 0.95–0.97, and these values have been adopted in the material card calibration to ensure conservative and safe finite element simulations.

Completing high-speed dynamic tensile testing on honeycomb sandwich materials and obtaining material performance parameters for both tension and compression are of significant importance for the subsequent benchmarking work of finite element simulation models.

4. Simulation Benchmarking of Honeycomb Sandwich Materials

With the development and increasing competitiveness in the automotive industry, the development cycles of automotive products are gradually shortening. Hence, CAE simulation technology is becoming increasingly crucial. For the accuracy of simulation analysis, precise material data is one of the important influencing factors [30]. The real stress–strain curve used in simulation analysis is typically obtained from tensile tests. According to current testing methods, the tensile curve can be divided into the elastic stage (I), uniform plastic deformation stage (II), diffuse necking stage (III), and local necking stage (IV) [31], as illustrated in Figure 8.

4.1. Material Process in Finite Element Method. Due to the calculation of engineering stress, which involves dividing the applied load by the initial cross-sectional area, as the test progresses and reaches the necking stage, the local cross-sectional area of the specimen rapidly decreases, leading to a drop in the applied load. This is reflected on the curve as a decrease in engineering stress. The relationship between engineering stress and engineering strain during the necking stage cannot accurately characterize the material's hardening behavior. Therefore, when processing data for simulation analysis, the extracted data corresponds to the true stress-true strain of the uniform plastic deformation stage [32].

$$\sigma_{true} = \sigma_{eng}\left(1 + \varepsilon_{eng}\right) \tag{1}$$

$$\varepsilon_{true} = \mathrm{In}\left(1 + \varepsilon_{eng}\right) \tag{2}$$

where σ_{eng} and ε_{eng} represent the stress and strain obtained from the aforementioned tensile test, respectively.

After the engineering stress and strain are processed, as shown in Figure 9, the real stress and strain are obtained, and the next step is to harden the material.

First, calculate the true stress–strain curve from the engineering stress–strain curve. Then, identify the yield point and remove the elastic section. In the LS-DYNA material card, the elastic section is calculated using the elastic modulus. After removing the elastic section, the descending part of the true stress–strain curve at yield is extended using the Swift–Hockett–Sherby (SHS) model, which is shown in Figure 10.

After the material curve undergoes hardening treatment, the next step involves conducting material damage and failure analysis.

4.2. Material Damage Failure Treatment and Integration. Conventional failure models are unable to simulate the material instability process. Damage calculation is often linearly cumulative, and the relationship between failure strain and stress triaxiality is monotonic. In contrast, the GISSMO failure model can simulate the material instability process. The damage calculation is nonlinear with exponential accumulation, and the relationship between failure strain and stress triaxiality can be non-monotonic [33]. It is a more realistic failure model.

This study considers the impact of material failure on simulation analysis. LS-DYNA provides a material damage failure criterion based on GISSMO [34], expressed by the following formula:

$$\Delta D = \frac{n}{\varepsilon_f(\eta)} D^{\left(1-\frac{1}{n}\right)} \Delta\varepsilon_p \tag{3}$$

Within the given formula, ΔD denotes the increment of damage variable; $\Delta\varepsilon_p$ denotes the equivalent plastic strain increment; n is the nonlinear cumulative damage index; and $\varepsilon_f(\eta)$ is the material fracture equivalent plastic strain related to the stress triaxiality, the value of which is obtained through experiments.

Beyond delineating the fracture behavior of materials under varying stress states, the GISSMO model also accounts for material instability during ductile fracture. The material's softening behavior is characterized by the variable F, expressed as follows:

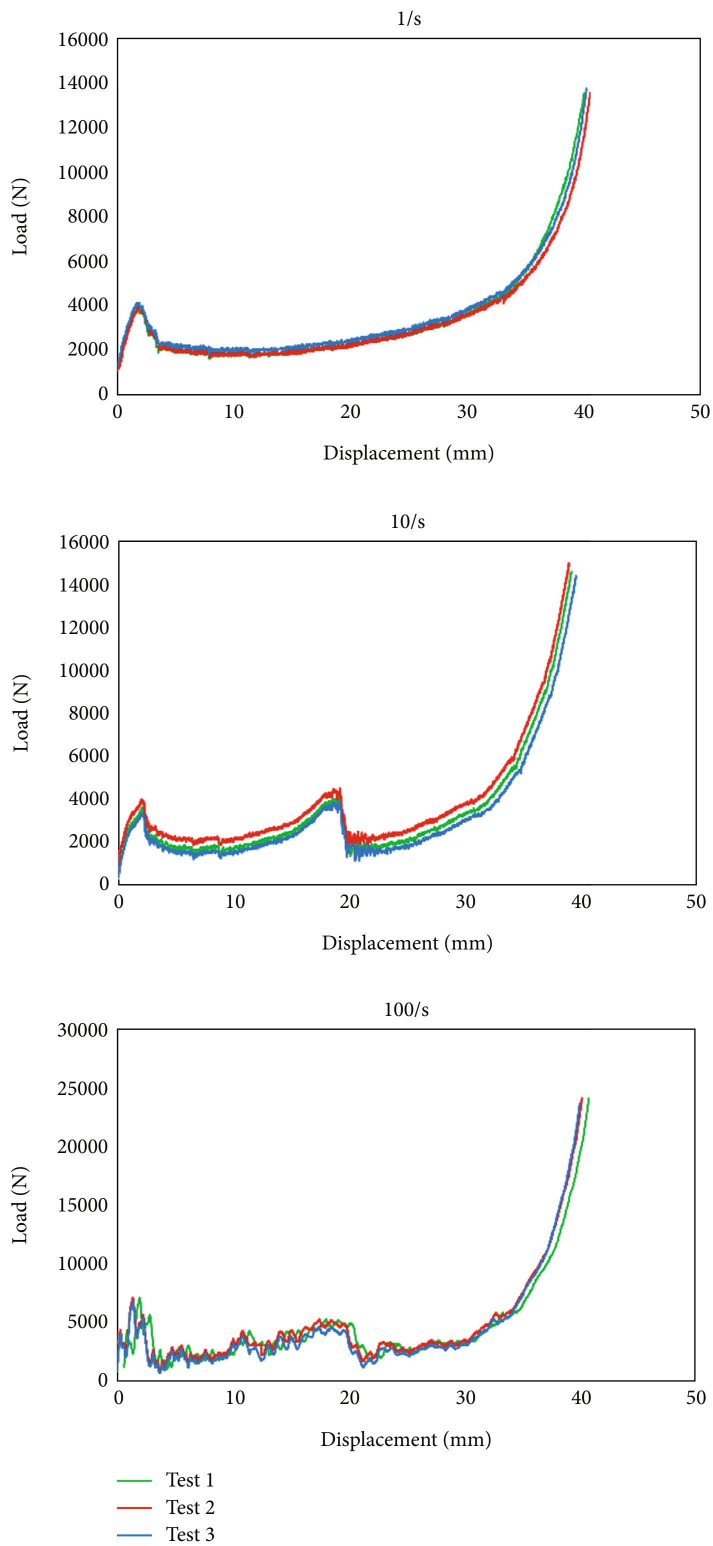

Figure 7: The stress–strain curve in compressive tests.

$$\Delta F = \frac{n}{\varepsilon_{crit}(\eta)} F^{\left(1-\frac{1}{n}\right)} \Delta\varepsilon_p \tag{4}$$

where F is the stability variable; ΔF is the stability variable increment; and $\varepsilon_{crit}(\eta)$ is the material critical equivalent plastic strain related to stress triaxiality, the value of which is obtained through parameter tuning by comparing simulation results with experimental data. Upon the unit's F value reaching 1, the stress begins to decrease. The formula for calculating the decreased stress is as follows.

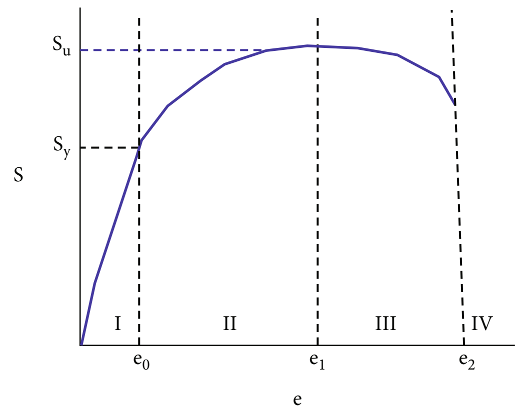

FIGURE 8: Different strain stages of material stretching.

$$\sigma^* = \sigma\left[1 - \left(\frac{D - D_{crit}}{1 - D_{crit}}\right)^m\right] \quad (5)$$

where $\sigma*$ is the post-softening stress; σ is the pre-softening stress; D_{crit} is the critical value of the variable D when $F = 1$; and m serves as the attenuation coefficient.

From the GISSMO material constitutive model, after conducting simulations and experiments for three-point bending, shearing, and tensile tests on material specimens, and aligning the results for benchmarking, stress–strain curves for the inner and outer layers of the sandwich material are obtained, as illustrated in the following Figures 11 and 12.

The obtained material curves are incorporated into the material cards of LS-DYNA and integrated into the overall vehicle finite element model, laying the groundwork for subsequent simulation analysis and optimization.

5. Analysis and Optimization of Safety Crash Performance of Sandwich Materials

5.1. Analysis of Frontal Collisions. The finite element modeling of the bus body was conducted using LS-DYNA, encompassing both the chassis and sandwich body structures to assess crashworthiness under frontal and rollover impact scenarios. The chassis frame, comprising longitudinal beams, cross members, and energy-absorbing elements, was discretized using shell and beam elements with appropriate mesh refinement in critical regions. The body structure was constructed using honeycomb sandwich panels, consisting of composite face sheets and foam-filled or paper-based core materials. Structural steel components were modeled using MAT_024 (Piecewise Linear Plasticity), with material parameters calibrated through high-speed tensile testing. The composite face sheets were characterized using MAT_187 (GISSMO), while the core was represented by either MAT_026 (honeycomb) and MAT_083 (crushable foam), based on results from dynamic compression tests. To enhance computational efficiency without compromising accuracy, small-scale features such as bolts and welds were idealized using spot weld constraints and tied contacts, and symmetry conditions were applied where appropriate. Simplified restraint systems and a rigid ground plane were employed to isolate structural response characteristics. This modeling framework effectively captured both global deformation patterns and localized material failure, with simulation results demonstrating strong agreement with experimental validation, thereby confirming the model's reliability for crash performance evaluation.

According to the Chinese National Standard "GB/T 1369-2020 Passenger Car Frontal Collision Occupant Protection," the bus undergoes a 100% frontal collision with a rigid wall at speeds of 30 to 32 km/h. The Hybrid-III 50% simulation dummy's injury criteria for the head, neck, chest, and thigh regions need to be satisfied. The finite element simulation model information is presented in Table 1.

The bus undergoes a 100% frontal collision with a rigid wall at a speed of 32 km/h, as illustrated in Figure 13.

5.2. Issues of FRB simulation. Analyzing the simulation results of the frontal collision, the upper body is a side structure made of honeycomb sandwich material, which is relatively stable during the collision. However, the lower body deforms greatly, and there are major problems with the structural design. The chassis structure of the bus is shown in Figure 14.

The simulation animation results of the frontal collision indicate significant deformation in the load-bearing structural beams of the chassis. This results in substantial compression of the occupant cabin survival space, causing the dummy's injury values to exceed the GBJTT1369-2020 regulatory limits; optimization is therefore required, as shown in Figures 15 and 16.

5.3. Optimization of FRB Simulation. The preliminary analysis reveals that the current energy absorption and force transmission performance is inadequate. Therefore, subsequent optimization efforts will primarily focus on improving the structural design and material selection of the lower body. The chassis structure of a bus plays a critical role in determining the transmission and distribution of collision energy during an impact event, which directly influences both vehicle deformation and occupant injury outcomes. Key factors include the architectural configuration of the chassis, the mechanical properties of the selected materials, and the design of the energy absorption pathways. An optimally engineered chassis structure can not only enhance the capacity to absorb impact energy but also facilitate the controlled transmission and dispersion of collision forces, thereby mitigating the severity of occupant injuries. The following outlines the main aspects of optimizing the chassis structure of a bus, as illustrated in Figure 17.

The optimization of the bus chassis structure is crucial for enhancing collision force transmission and occupant protection. The chassis serves as the foundational load-bearing framework, and its design plays a decisive role in

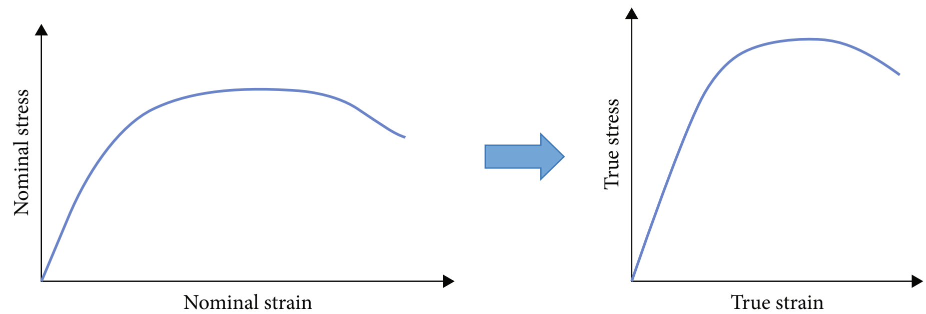

Figure 9: Conversion of engineering stress and strain to true stress and strain.

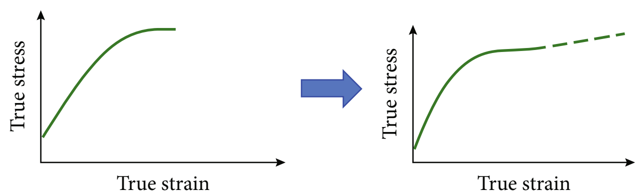

Figure 10: Hardening process of material curve.

guiding and distributing impact forces during a collision. A well-engineered chassis (as shown in Figure 18) must exhibit sufficient stiffness to limit excessive deformation, thereby maintaining the integrity of the passenger compartment and preventing intrusions that could lead to severe or fatal injuries.

Inadequate structural rigidity in the lower body may result in uncontrolled deformation and force concentrations that compromise occupant safety. To mitigate this, the transmission path of collision forces must be deliberately designed to redirect energy toward structurally reinforced components-such as the front longitudinal beams, door sill reinforcements, and cross members—thereby avoiding direct impact on the occupant space. In this study, the force transmission capability of the bus chassis was improved by integrating additional structural elements into the lower body. These components work synergistically to disperse and redirect collision forces toward the rear structure, enhancing energy dissipation and reducing localized stress concentrations; the results are shown in Figures 19 and 20.

The baseline bus simulation model exhibited a maximum crush depth of 396 mm. Following structural optimization, the deformation was substantially reduced to 142.6 mm, significantly improving the driver's survival space. A comparative analysis of the dummy injury metrics before and after optimization is presented in Table 2.

From Table 2, it can be observed that in the baseline simulation model, there is a slight collision between the dummy's head and the steering wheel, resulting in a higher head injury criterion (HIC) and increased risk. After optimization, the HIC for the dummy's head is reduced to 263 by 100 ms, indicating minimal deformation in the survival space structure of the occupant cabin after the collision. The distance between the dummy and the steering wheel is increased, leading to a significant improvement in safety.

5.4. Analysis of Rollover Collision. The core optimization strategy for bus rollover performance, as defined by ECE Regulation R66, emphasizes enhancing the structural integrity and crashworthiness of the vehicle during rollover events. This approach is fundamentally guided by two critical objectives: the preservation of occupant survival space and the enhancement of energy absorption capacity through the application of honeycomb sandwich materials.

Firstly, maintaining sufficient survival space is critical in minimizing the risk of fatal injuries during a rollover. As illustrated in Figure 21, the structural design must ensure that the deformation of the vehicle body does not intrude into the designated survival zone, particularly in the driver and main passenger areas. Preserving this space is essential for preventing direct contact between collapsing structures and occupants, thereby significantly reducing the severity of injuries.

Secondly, sandwich composite materials were integrated into the upper body structures (highlighted in pink in Figure 22) to enhance energy absorption efficiency.

These materials, typically composed of high-strength outer face sheets and a lightweight foam or honeycomb core, exhibit superior deformation behavior and energy dissipation performance compared to conventional structural materials. As illustrated in Figure 23, the sandwich structure functions analogously to a large spring, compressing progressively under load and effectively absorbing and distributing the impact energy. This spring-like behavior plays a crucial role in mitigating peak forces during rollover events, thereby enhancing the structural resilience and overall safety performance of the bus.

Under rollover loads, the core material undergoes progressive compression and shear, while the outer skins provide structural stiffness and limit excessive deflection. This combination enables effective distribution and attenuation of impact forces, helping to prevent sudden structural collapse and enhancing the bus's ability to maintain structural integrity during rollover scenarios. The use of sandwich structures also contributes to vehicle lightweighting while meeting safety requirements, making them a key element in the structural optimization process.

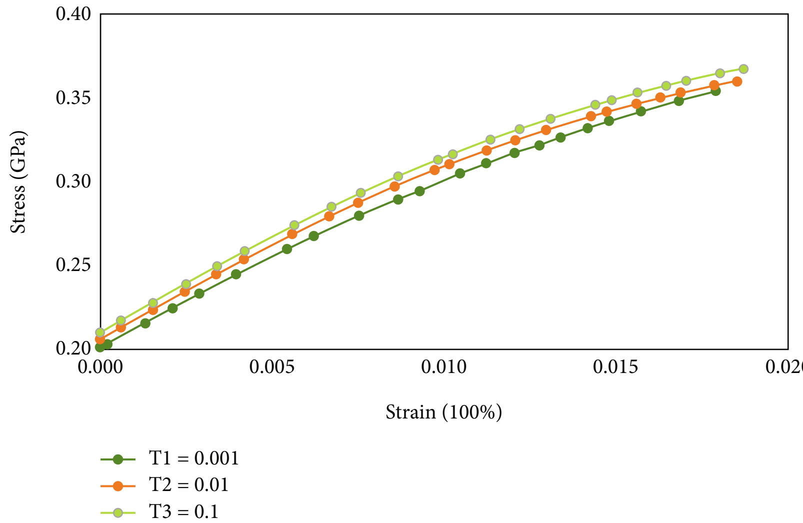

Figure 11: Stress–strain curve of inner structure.

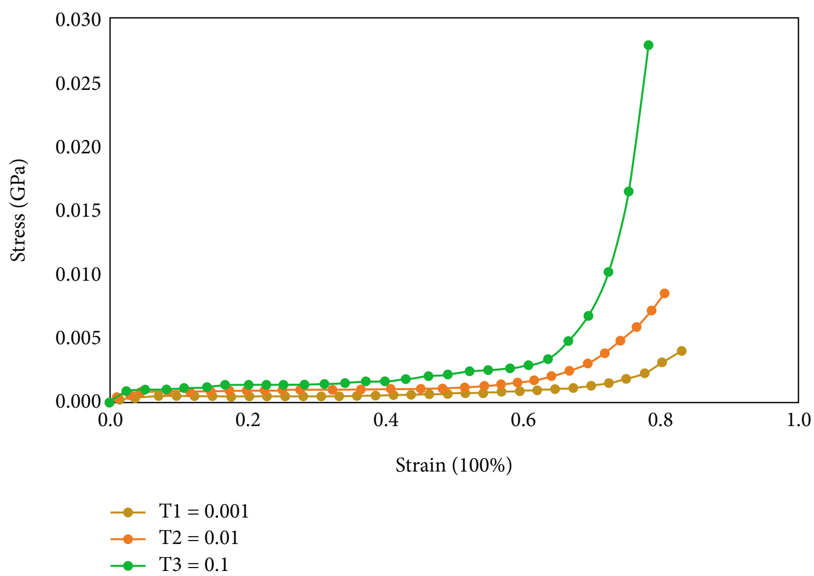

Figure 12: Stress–strain curve of outer structure.

TABLE 1: Bus simulation model.

Item	Parameter data
Solution software	LS-DYNA R13
Regulation	GBJTT1369-2020
Analysis condition	Frontal 100% overlap collision (FRB)
Collision speed	32Km/h
(length/width/height)	7589 × 2450 × 2737 (mm)
Mass	6668 (kg)
Element number	6,800,000
Dummy	Hybrid III 50%

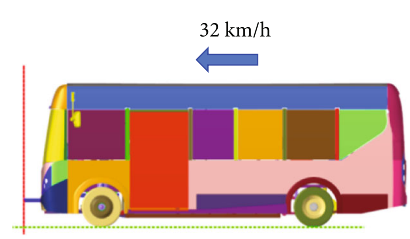

Figure 13: FRB simulation model.

The certification process defined by the United Nations Economic Commission for Europe (UN-ECE) Regulation R66 outlines the safety testing requirements for evaluating the structural integrity of buses under side rollover conditions. In this study, the relevant parameters were derived through analytical formulas and subsequently applied in the finite element software LS-DYNA to obtain simulation results.

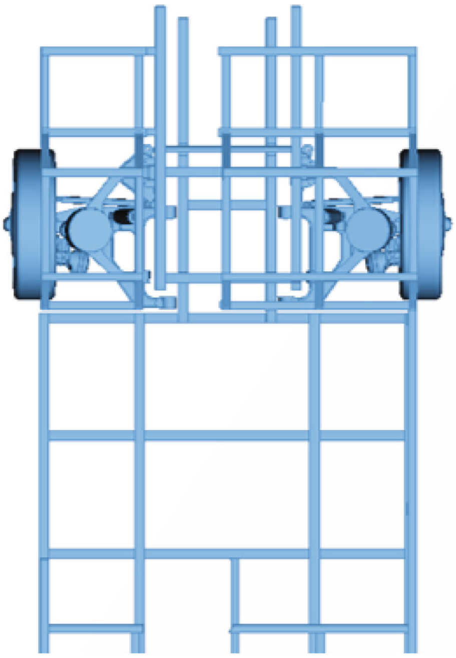

FIGURE 14: Original bus chassis.

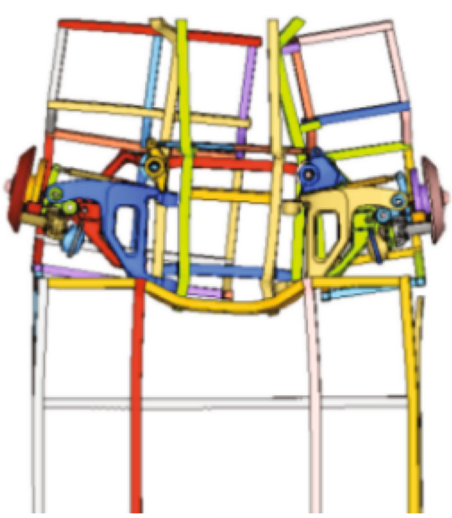

FIGURE 15: Chassis deformation at 120 ms.

FIGURE 16: Dummy dynamics at 120 ms.

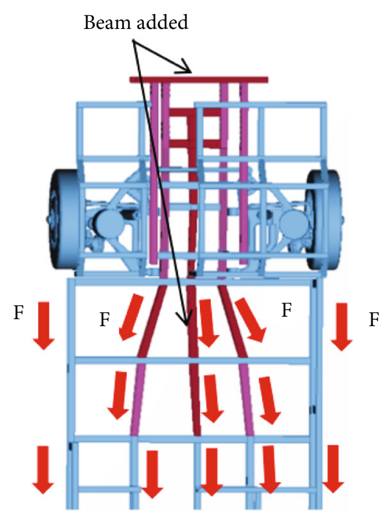

FIGURE 17: Force distribution of the optimized chassis structure.

In Figure 24, CG represents the center of gravity of the bus, A is the distance from the rotation axis to the longitudinal vertical center plane of the bus, B is the distance from the center of gravity of the bus to the longitudinal vertical center plane, h0 is the initial height of the center of gravity of the bus on the rollover platform, and h1 is the height of the center of gravity of the bus at the critical rollover point.

From the critical rollover position to the process of contacting the ground, the center of gravity dropped by $\triangle h$ = 970 mm. At the time of rollover, the angular velocity of the flip platform and the bus remained constant at 5°/s, or 0.087 rad/s. According to the law of conservation of energy, the kinetic energy plus the gravitational potential energy at the critical rollover moment is equal to the kinetic energy plus the gravitational potential energy at the time of contacting the ground, that is,

$$E_{K1} + E_{P1} = E_{K2} + E_{P2} \tag{6}$$

$$\frac{1}{2} J\omega_1^{\ 2} + mgh_1 = \frac{1}{2} J\omega_2^{\ 2} + mgh_2 \tag{7}$$

$$\frac{1}{2} J\left(\omega_2^{\ 2} - \omega_1^{\ 2}\right) = mg\Delta h \tag{8}$$

$$J = \frac{2mg\Delta h}{\omega_1^{\ 2} - \omega_2^{\ 2}} \tag{9}$$

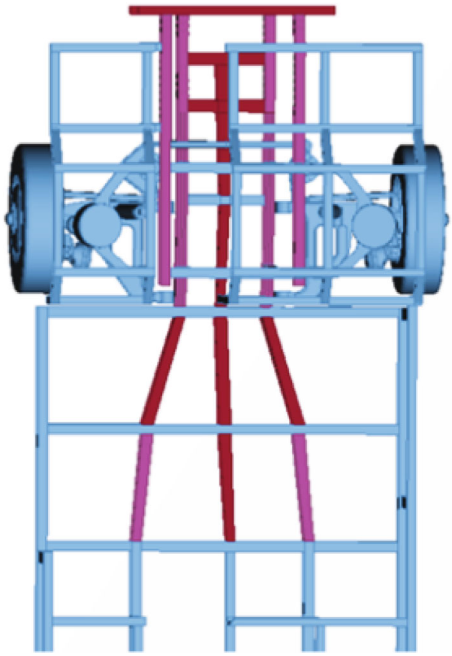

Figure 18: Optimization of chassis structure.

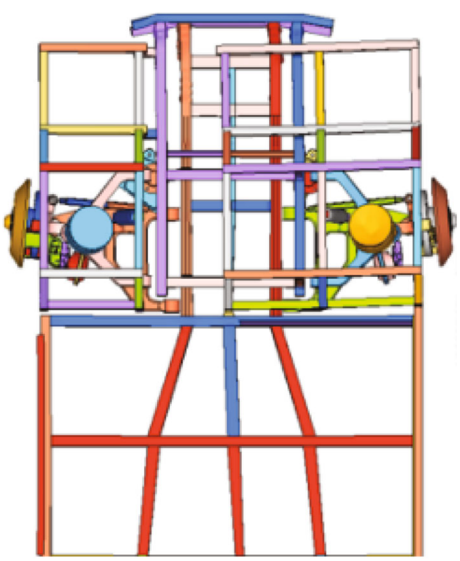

Figure 19: Optimized chassis deformation at 120 ms.

where E_{K1} is the kinetic energy at the critical rollover moment, E_{P1} is the potential energy at the critical rollover moment, E_{K2} is the kinetic energy at the time of contact with the ground, E_{P2} is the potential energy at the time of contact with the ground, J is the moment of inertia of the whole vehicle, h_1 is the height of the center of gravity of the whole vehicle from the ground at the critical rollover moment, and h_2 is the height of the center of gravity of the whole vehicle from the ground at the time of contact with the ground, and ω_1 is the angular velocity of the flip platform, which is 0.087 rad/s.

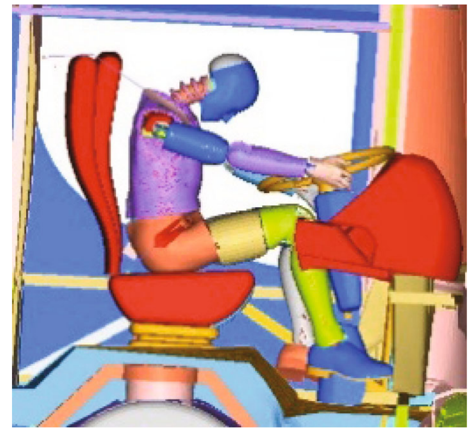

Figure 20: Dummy dynamics at 120 ms after optimization.

TABLE 2: Results before and after model optimization.

Hybrid-III 50% dummy	GBJTT1369-2020	Original model	Optimize model
Head	HIC < 500	956	63
Neck	My < 57 N·m	35	30
Chest	Acceleration < 30 g	42	15
Leg	Fz < 10(KN)	3	2

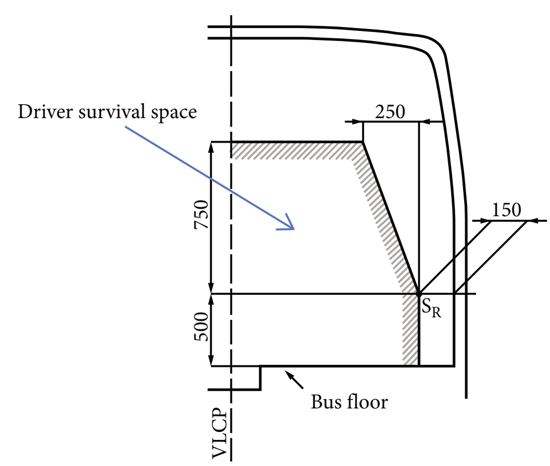

Figure 21: Schematic diagram of driver survival space.

Set the value of any angle and import the model into LS-DYNA for calculation. The value of initial kinetic energy E_{K0} can be calculated in LS-DYNA, from

$$E_{K0} = \frac{1}{2} J \omega_0{}^2 \tag{10}$$

Obtained:

$$J = \frac{2E_{K0}}{\omega_0{}^2} \tag{11}$$

Figure 22: Upper bus body structure of sandwich material.

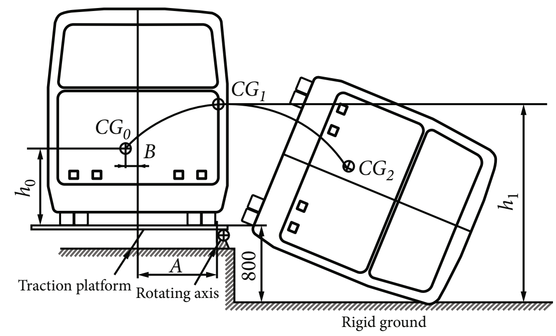

Figure 24: Rollover collision diagram.

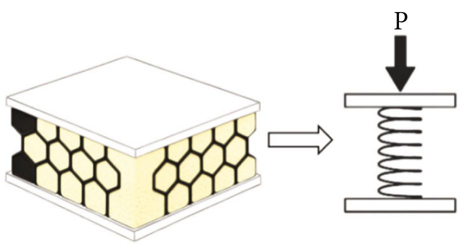

Figure 23: Working principle of sandwich material.

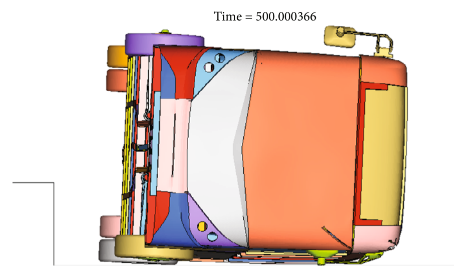

Figure 25: Bus deformation at 500 ms.

Substituting J into Equation (11) yields the angular velocity ω_2. Substitute the obtained angular acceleration value ω_2 into the loading keyword of LS-DYNA (*INITIAL_VELOCITY_GENERATION) to obtain the following simulation results. The finite element simulation model for the side rollover scenario was computed up to 500 ms, capturing the complete dynamic response of the structure. The time-history animation results of the rollover process are presented in Figure 25.

As illustrated in Figure 26, the deformation of the bus driver's cabin structure in the lateral (width) direction is approximately 100 mm, while the rear body structure experiences a deformation of about 95 mm—both well within the regulatory limit of 250 mm. Despite these deformations, the overall structural integrity of the bus body remains intact, with minimal intrusion into the passenger compartment. The occupant protection space is effectively preserved, demonstrating that adequate survival space is maintained throughout the rollover event.

According to the rollover assessment criteria specified in ECE Regulation R66, the simulation results indicate that the bus structure successfully meets the rollover safety requirements.

5.5. Experimental Validation of Frontal and Rollover Collisions. After completing the material characterization, simulation analysis, and structural optimization for the frontal rigid barrier (FRB) impact scenario in accordance with the GB standard, as well as the rollover scenario based on ECE Regulation R66, the next phase involved experimental validation. Physical crash tests were conducted to verify the accuracy of the simulation results and confirm that the vehicle meets the required safety performance under both frontal and rollover conditions.

Following the fabrication of two prototype vehicles, full-scale experiments were carried out in a controlled laboratory environment, with the entire process documented through photographs. Figure 27 shows the structural condition of the sandwich-material bus body after the 100% frontal collision test.

Figure 28 presents the post-test condition of the bus body structure after the rollover experiment. In both test scenarios, the observed structural deformations were minimal and demonstrated strong consistency with the predictions from the optimized simulation models, thereby confirming the validity and effectiveness of the proposed lightweight design approach.

The application of honeycomb sandwich materials in the vehicle body results in a weight reduction of approximately 500 kg compared to traditional steel and aluminum structures. At the same time, these materials demonstrate excellent crash safety performance. Moreover, the overall manufacturing cost and market pricing remain comparable to those of conventional steel and aluminum materials. Given this combination of lightweight, safety, and economic feasibility, honeycomb sandwich structures hold significant potential for widespread adoption in the future automotive market.

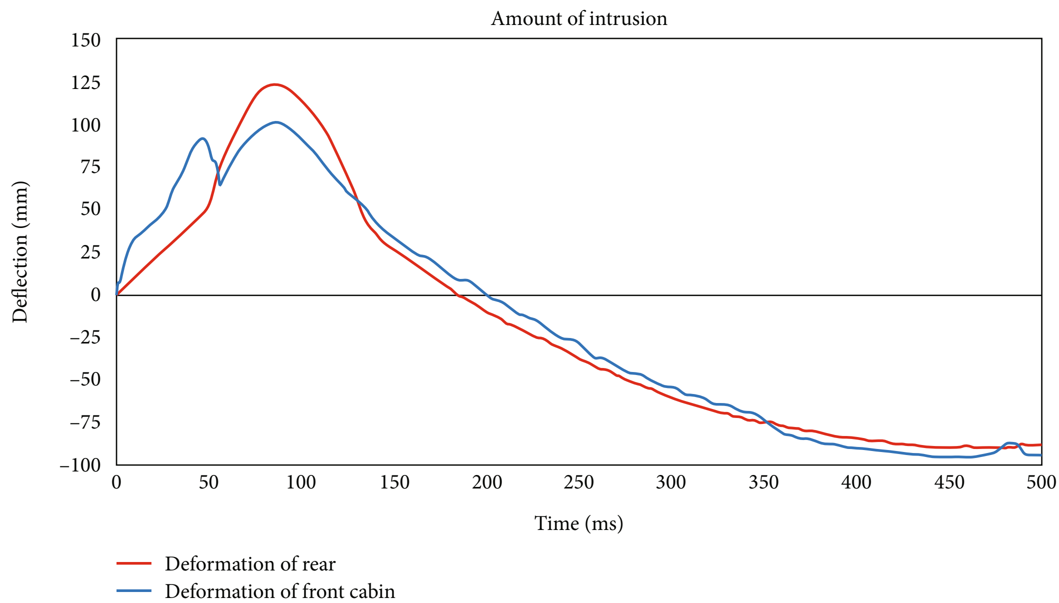

Figure 26: Intrusion curve of frontal and rear.

Figure 27: Sandwich body after FRB test.

Figure 28: Sandwich body after R66 test.

6. Conclusions

This study investigates the crashworthiness of the bus chassis longitudinal beam structure and the bus body of honeycomb sandwich materials. Based on the analysis and experimental validation, the following conclusions were drawn:

1. High-speed dynamic tensile and compression testing was conducted to obtain the engineering stress–strain curves of the materials, which were subsequently converted into true stress–strain curves. Based on the material hardening behavior, the GISSMO damage constitutive model was selected to accurately capture failure characteristics. The resulting material parameters were used to create precise material cards, which were integrated into the LS-DYNA full-vehicle finite element model for crashworthiness simulation. This approach provides valuable technical support for the research and development of bus body of sandwich material.

2. In the frontal crash scenario, as defined by the Chinese national standard GB JTT 1369-2020, the crashworthiness of the bus was primarily enhanced through optimization of the chassis load-bearing beam, which serves as the main force transmission path. In contrast, under the rollover condition governed by the European regulation ECE-R66, the stability and energy-absorbing performance of the honeycomb sandwich bus body structure played a decisive role. Finite element simulations and physical tests confirmed that the optimized chassis and body designs effectively maintained structural integrity, preserved occupant survival space, and significantly improved overall crash performance.

3. This study proposes a novel methodology that combines structural optimization, high-fidelity material modeling, and experimental validation to advance the design of lightweight and crashworthy electric buses. By optimizing the chassis for frontal impacts and employing honeycomb sandwich materials to enhance rollover performance, the approach ensures

regulatory compliance while achieving significant weight reduction and improved energy efficiency. The integrated framework offers a robust reference for future developments in safe and sustainable electric bus design.

Data Availability Statement

The data that support the findings of this study are available from the corresponding author upon reasonable request.

Conflicts of Interest

The authors declare no conflicts of interest.

Author Contributions

Yi Pang, Sai Zhang, Pengfei Ren: conceptualization, analysis, methodology, and writing—original draft. Shaw Voon Wong, Yong Han, Yahaya bin Ahmad, Kean sheng Tan, Azizan As'arry: supervision, resources, project administration, and writing—review and editing.

Funding

This study is supported by the Xiamen City Natural Science Foundation, 3502Z20227223, and the Industry Technology Project by the Fujian Province Department, 2022G43 2023G048.

Acknowledgments

The authors would like to thank the China Automotive Technology and Research Center and Hong Kong Sunny Motors for their experimental support.

References

[1] Q. Q. Li, E. Li, T. Chen, L. Wu, G. Q. Wang, and Z. C. He, "Improve the Frontal Crashworthiness of Vehicle Through the Design of Front Rail," *Thin-Walled Structures* 162 (2021): 107588, https://doi.org/10.1016/j.tws.2021.107588.

[2] L. Hu, X. Bao, M. Lin, C. Yu, and F. Wang, "Research on Risky Driving Behavior Evaluation Model Based on CIDAS Real Data," *Proceedings of the Institution of Mechanical Engineers, Part D: Journal of Automobile Engineering* 235, no. 8 (2021): 2176–2187, https://doi.org/10.1177/0954407020985972.

[3] H. Y. Ko, K. B. Shin, K. W. Jeon, and S. H. Cho, "A Study on the Crashworthiness and Rollover Characteristics of Low-Floor Bus Made of Sandwich Composites," *Journal of Mechanical Science and Technology* 23, no. 10 (2009): 2686–2693, https://doi.org/10.1007/s12206-009-0731-7.

[4] UN Economic Commission for Europe, Regulation No. 66: Uniform technical prescriptions concerning the approval of large passenger vehicles with regard to the strength of their superstructure, Geneva, Switzerland, 2006.

[5] S. M. R. Hashemi, A. C. Waltona, and K. Kayvantash, "Strength of Super-Structure UN-ECE R66 Rollover Approval of Coaches Based on Thin-Walled Framework Structures," *International Journal of Vehicle Structures and Systems* 1, no. 4 (2009): 78–84, https://doi.org/10.4273/ijvss.1.4.04.

[6] National Automobile Standardization Technical Committee Passenger Car Branch, JT/T 1369-2020: Occupant protection in bus frontal collision, issued by the Ministry of Transport of the People's Republic of China, Beijing: Standards Press of China, Dec. 2020.

[7] J. Long, Z. Yuan, X. Fu, and S. Zhou, "A Research on the Body Lightweighting of an Extended-Range Electric Vehicle Based on Frontal Crash Safety," *Qiche Gongcheng/Automotive Engineering* 37, no. 4 (2015): 466–471.

[8] R. Sankaranarayanan, N. R. J. Hynes, M. P. Nikolova, and J. B. Królczyk, "Self-Pierce Riveting: Development and Assessment for Joining Polymer—Metal Hybrid Structures in Lightweight Automotive Applications," *Polymers, Review* 15, no. 20 (2023): 4053, https://doi.org/10.3390/polym15204053.

[9] G. Li and X. Liu, "Literature Review on Research and Development of Automotive Lightweight Technology," *Cailiao Kexue yu Gongyi/Material Science and Technology, Review* 28, no. 5 (2020): 47–61, https://doi.org/10.11951/j.issn.1005-0299.20190232.

[10] Y. Wang and G. Hu, "Research Progress of Improving Surface Quality of Microcellular Foam Injection Parts," *Applied Mechanics and Materials* 66-68 (2011): 2010–2016, https://doi.org/10.4028/www.scientific.net/AMM.66-68.2010.

[11] A. Cimprich, K. Sadayappan, and S. B. Young, "Lightweighting Electric Vehicles: Scoping Review of Life Cycle Assessments," *Journal of Cleaner Production, Review* 433 (2023): 139692, https://doi.org/10.1016/j.jclepro.2023.139692.

[12] J. M. Boileau, S. das, A. Deb, et al., "List of Contributors," in *Materials, Design and Manufacturing for Lightweight Vehicles*, ed. P. K. Mallick (Woodhead Publishing, Second edition, 2021), https://doi.org/10.1016/B978-0-12-818712-8.00016-1.

[13] A. Zvorykina, O. Sherepenko, M. Neubauer, and S. Jüttner, "Dissimilar Metal Joining of Aluminum to Steel by Hybrid Process of Adhesive Bonding and Projection Welding Using a Novel Insert Element," *Journal of Materials Processing Technology* 282 (2020): 116680, https://doi.org/10.1016/j.jmatprotec.2020.116680.

[14] T. Hata, Y. Iwata, H. Takahashi, and M. Murakami, "Development of Aluminum Die-Casting Global Material Specifications for Front Subframe," *Keikinzoku/Journal of Japan Institute of Light Metals* 72, no. 4 (2022): 144–150, https://doi.org/10.2464/jilm.72.144.

[15] S. H. Hao and R. Hu, "Optimal Design of the All - Aluminum Alloy Body Roof Frame of Hybrid Electric Bus," *Automotive Technology* 6 (2016): 11–15.

[16] S. C. Pinto, N. H. Silva, R. J. Pinto, et al., "Multifunctional Hybrid Structures Made of Open-Cell Aluminum Foam Impregnated With Cellulose/Graphene Nanocomposites," *Carbohydrate Polymers* 238 (2020): 116197, https://doi.org/10.1016/j.carbpol.2020.116197.

[17] X. Xu, Y. Zhang, X. Wang, J. Fang, J. Chen, and J. Li, "Searching Superior Crashworthiness Performance by Constructing Variable Thickness Honeycombs With Biomimetic Cells," *International Journal of Mechanical Sciences* 235 (2022): 107718, https://doi.org/10.1016/j.ijmecsci.2022.107718.

[18] A. Cui, F. Liu, H. Zhang, Y. Hao, C. Chen, and R. Zhang, "Performance Analysis and Optimization of Foam-filled Aluminum-Alloy Corrugated Sandwich Panel Structure for Vehicle Body," *Qiche Gongcheng/Automotive Engineering* 41, no. 10 (2019): 1221–1227, https://doi.org/10.19562/j.chinasae.qcgc.2019.010.017.

[19] V. Volpe, S. Lanzillo, G. Affinita, B. Villacci, I. Macchiarolo, and R. Pantani, "Lightweight High-Performance Polymer Composite for Automotive Applications," *Polymers* 11, no. 2 (2019): 326, https://doi.org/10.3390/polym11020326.

[20] Y. G. T. Girijappa, V. Ayyappan, M. Puttegowda, S. M. Rangappa, J. Parameswaranpillai, and S. Siengchin, "Plastics in Automotive Applications," in *Encyclopedia of Materials: Plastics and Polymers*, ed. M. S. J. Hashmi (Elsevier, 2022), 103–113, https://doi.org/10.1016/B978-0-12-820352-1.00052-3.

[21] N. Fuenmayor, M. Shah, and T. Glogovsky, "Breaking New Ground With Thermoplastic Polyolefin Body Panels," in *Proceedings of the 11th-Annual SPE TPO Conference - World's Leading Automotive Olefins Forum* (Society of Plastics Engineers, 2009).

[22] N. Krishnamoorthy, S. Nayak, G. K. Surisetty, M. Chaturvedi, and S. Shuler, "Polycarbonate Glazing Body Panels for Automotive Applications" SAE Technical Paper 2009-26-0085, 2009. https://doi.org/10.4271/2009-26-0085.

[23] S. K. Juikar and S. G. Warkar, "Biopolymers for Packaging Applications: An Overview," *Packaging Technology and Science, Review* 36, no. 4 (2023): 229–251, https://doi.org/10.1002/pts.2707.

[24] B. Myrold, O. Jensrud, and J. Holmestad, "Investigation of the Formability of AA6010 in an Integrated Forming and Hardening Process Aiming to Reduce the Energy Consumption in High Volume Production of Automotive Components," *Metals* 13, no. 11 (2023): 1877, https://doi.org/10.3390/met13111877.

[25] G. Sathishkumar, P. Sathiya, and S. Senthil Murugan, "Evaluation of Mechanical and Microstructural Properties of High-Temperature Hastelloy X Alloy-Welded Joints Made by Laser Welding Process," *Journal of Testing and Evaluation* 51, no. 6 (2023): 3947–3967, https://doi.org/10.1520/JTE20220653.

[26] J. Deng, Z. Li, W. Jiang, D. C. Liu, J. He, and B. Li, "Selective Volatilization and Recovery of Valuable Metals by Vacuum Carbothermal Reduction of Copper Anode Slime," *JOM* 75, no. 9 (2023): 3489–3500, https://doi.org/10.1007/s11837-023-05996-z.

[27] N. Vilchez, M. Ortega Varela de Seijas, A. Bardenhagen, T. Rohr, and E. Stoll, "A Novel Induction Heater for Sintering Metal Compacts With a Hybrid Material Extrusion Device," *Electronics* 12, no. 14 (2023): 3033, https://doi.org/10.3390/electronics12143033.

[28] B. Ildefonso and D. Storer, "State-of-the-Art Analysis on Alternative Materials for the Automotive Industry," *Transportation Research Procedia* 72 (2023): 1560–1567, https://doi.org/10.1016/j.trpro.2023.11.624.

[29] J. Zheng, H. Li, and J. D. Hogan, "Strain-Rate-Dependent Tensile Response of an Alumina Ceramic: Experiments and Modeling," *International Journal of Impact Engineering* 173 (2023): 104487, https://doi.org/10.1016/j.ijimpeng.2022.104487.

[30] M. Pietrzyk, L. Madej, L. Rauch, and D. Szeliga, *Computational Materials Engineering: Achieving High Accuracy and Efficiency in Metals Processing Simulations* (Butterworth-Heinemann, 2015).

[31] C. T. Herakovich, "Mechanics of Composites: A Historical Review," *Mechanics Research Communications* 41 (2012): 1–20, https://doi.org/10.1016/j.mechrescom.2012.01.006.

[32] M. Luo and T. Wierzbicki, "Numerical Failure Analysis of a Stretch-Bending Test on Dual-Phase Steel Sheets Using a Phenomenological Fracture Model," *International Journal of Solids and Structures* 47, no. 22-23 (2010): 3084–3102, https://doi.org/10.1016/j.ijsolstr.2010.07.010.

[33] T. Zhu, H. Ding, C. Wang, et al., "Parameters Calibration of the GISSMO Failure Model for SUS301L-MT," *Chinese Journal of Mechanical Engineering* 36, no. 1 (2023): 20, https://doi.org/10.1186/s10033-023-00844-2.

[34] C. Y. Xu, J. C. Zhang, and C. W. Lian, "Study on Fracture Failure Behavior of DH590 High Strength Steel Based on GISSMO Damage Model," *Suxing Gongcheng Xuebao/Journal of Plasticity Engineering* 28, no. 6 (2021): 68–74, https://doi.org/10.3969/j.issn.1007-2012.2021.06.009.